How Crystal Symmetry Dictates Non-Local Vibrational Circular Dichroism in the Solid State

Sascha Jähnigen, Katia Le Barbu-Debus, Régis Guillot, Rodolphe Vuilleumier, Anne Zehnacker

Chirality

How to cite:
International Edition: doi.org/10.1002/anie.202215599
German Edition: doi.org/10.1002/ange.202215599

How Crystal Symmetry Dictates Non-Local Vibrational Circular Dichroism in the Solid State

Sascha Jähnigen, Katia Le Barbu-Debus, Régis Guillot, Rodolphe Vuilleumier, and Anne Zehnacker**

Abstract: Solid-State Vibrational Circular Dichroism (VCD) can be used to determine the absolute structure of chiral crystals, but its interpretation remains a challenge in modern spectroscopy. In this work, we investigate the effect of a twofold screw axis on the solid-state VCD spectrum in a combined experimental and theoretical analysis of $P2_1$ crystals of (*S*)-(+)-1-indanol. Even though the space group is achiral, a single proper symmetry operation has an important impact on the VCD spectrum, which reflects the supramolecular chirality of the crystal. Distinguishing between contributions originating from molecular chirality and from chiral crystal packing, we find that while IR absorption hardly depends on the symmetry of the space group, the situation is different for VCD, where completely new non-local patterns emerge. Understanding the two underlying mechanisms, namely gauge transport and direct coupling, will help to use VCD to distinguish polymorphic forms.

Introduction

The importance of chirality in drug design and activity is well recognised,[1,2] but at the same time pharmaceutical industry often deals with solids whose properties affect bioavailability and developability of potential drug candidates.[3] Thorough characterisation of chiral solid substances and of their various forms (polymorphs, hydrates, etc.) is therefore one crucial step in modern pharmaceutical development processes.[4] This may be achieved using NMR spectroscopy or diffraction techniques, especially X-ray diffraction (XRD),[4,5] whereas single-crystal XRD is the most rigorous way to provide full chiral information. Yet, single crystals can be inaccessible or not representative of the full sample. Powder diffraction, in turn, does not yield the absolute structure of the chiral sample due to the isotropic experimental conditions.

In this context, chiroptical spectroscopy provides an increasingly important, cost-effective alternative for the study of chiral solids,[6–10] even though it delivers only implicit information about the molecular configuration and often requires computational interpretation. In recent years, vibrational circular dichroism (VCD) has come into focus, which is a ground-state property relying on a wealth of absorption bands (in the infrared region), many more than its electronic counterpart.[11] Being a very sensitive probe of molecular conformation and environment, VCD has been applied to a wide range of molecules including natural products, host-guest systems, peptides and proteins, nanoparticles or catalysts,[12–21] supramolecular organisation in the condensed phase,[8,22–32] and the formation of chiral phases from achiral subunits.[5,33,34] In particular, the utility of solid-state VCD for the resolution of molecular chirality and supramolecular chirality has been noted by Sato and co-workers.[35–37] VCD is distinguished from electronic circular dichroism by the fact that it directly addresses vibrational transitions in the supramolecular chiral framework, such as functional groups connected by covalent or non-covalent interactions (hydrogen bonds etc.).[36,37] Therefore, the identification of enantiomorphisms in the crystal structure—at constant IR absorption—is a key feature of solid-state VCD, which can be used to distinguish polymorphic forms, as demonstrated in several seminal works.[8,37–40]

A VCD spectrum of a molecule in solid state is very different from one measured in solution. In the crystal, the molecules are closely packed and the conformational flexibility is dramatically reduced, which prevents conformational averaging of signals. Another consequence is a stable supramolecular connection of the molecules giving rise to delocalised vibrational modes and thereby to non-local VCD contributions stemming from the chiral crystal.[36,41,42]

[*] S. Jähnigen, R. Vuilleumier
PASTEUR, Département de Chimie, Ecole Normale Supérieure, CNRS, PSL University, Sorbonne Université
75005 Paris (France)
E-mail: sascha.jahnigen@ens.psl.eu

K. Le Barbu-Debus, A. Zehnacker
Institut des Sciences Moléculaires d'Orsay (ISMO), CNRS, Université Paris-Saclay
91405 Orsay (France)
E-mail: anne.zehnacker-rentien@universite-paris-saclay.fr

R. Guillot
Institut de Chimie Moléculaire et des Matériaux d'Orsay (ICMMO), CNRS, Université Paris-Saclay
91405 Orsay (France)

Solid-state VCD thus bears plenty of meaningful information, yet it requires a careful experimental protocol in order to avoid spectral artefacts from the solid sample.[43,44] In addition, the necessary reference calculations have to suitably account for the supramolecular arrangement of molecules in the crystal. Conventional static DFT calculations applied to isolated molecules or molecular clusters have been successfully used to approximate the system through sub-units extracted from the crystal structure,[5,25,31,32,34,45–47] but this has limited applicability: Boundary effects stemming from the finite size model can substantially alter the frequencies or add artefacts to the spectrum.[24] The result otherwise depends on how well a small cluster describes the crystal. To some extent, it may account for the delocalisation of local vibrational modes and the non-local IR and VCD intensity enhancement due to coupling between molecules. However, it has been shown by means of fully periodic quantum calculations that, for instance, in alanine crystals the observed VCD enhancement was due to long-range effects related to helical arrangement of oscillators, which is difficult to capture with a small cluster.[41,48]

The development of tools for the computation of VCD has made great progress in recent years. On one hand, there is the ever increasing accessibility of the two quantum theoretical formulations in order to compute the electronic contribution to the magnetic dipole moments: magnetic field perturbation theory (MFPT)[49,50] and nuclear velocity perturbation theory (NVPT).[51,52] MFPT is now available in many software packages[50,53,54] and is widely used for DFT-based static calculations of VCD resting on harmonic normal modes. NVPT, in turn, can efficiently be coupled to molecular dynamics simulations and bulk phase scenarios.[41,55,56] Very recently, MFPT and NVPT have also been implemented into the CP2K package and a direct comparison of the two methods is provided.[57] On the other hand, anharmonicity or the extension of structural models to mimic bulk scenarios are becoming practicable.[10,56,58–64] In particular, ab initio molecular dynamics (AIMD), though relying on classical nuclear mechanics, offer a workable route to post-harmonic studies of bulk phase systems, including crystals.[42,65–70] The IR and VCD spectra are directly obtained from time-correlation functions (TCF), which yield a continuous line shape function with peak shapes determined by temperature effects and the thorough sampling of shallow potential energy surfaces.[66,71,72] Still, solid-state computations of VCD including full periodicity have long been considered unfeasible in view of not knowing the correct treatment of the magnetic gauge; only recently this hurdle has been overcome by our group,[42] and the corresponding tools are accessible through the *ChirPy* package.[73]

Crystals formed by chiral molecules contain only proper symmetry operations (translations, rotations, and combinations thereof) and therefore belong to the Sohncke space groups. The most common are monoclinic $P2_1$ and orthorhombic $P2_12_12_1$.[74] Interestingly, these space groups, which contain only twofold rotations, are actually achiral (i.e., non-enantiomorphic) and can be superposed with their mirror images. The chirality introduced by the asymmetric unit, however, transforms through the lattice to form truly chiral crystals.[75] Sato, Miyata, and co-workers have described the mechanism of chirality generation by twofold rotation and the connection between the two levels of chirality, one stemming from the asymmetric unit itself and the other bound to the chiral crystal packing.[36,37,76]

In this article, the VCD spectrum of monoclinic (*S*)-(+)-1-indanol crystals with $P2_1$ symmetry (Scheme 1) is analysed in detail. While there can be little doubt *that* VCD patterns arise from supramolecular organisation, it is still obscure *how* these patterns arise and what the role of symmetry is.[41,42] We interpret the experimental data by means of fully periodic quantum calculations based on AIMD-NVPT and XRD data, and discuss non-local VCD signatures stemming from the chiral crystal structure. We show how a simple achiral twofold screw axis gives rise to purely non-local VCD patterns based on the two different mechanisms, gauge transport (GT) and direct coupling (DC). On the way, we analyse the capability of static calculations of a simple cluster model based on normal modes and MFPT to account for these non-local effects.

Results and Discussion

(*S*)-(+)-1-Indanol crystallises in the Sohncke group $P2_1$, whose only symmetry element is a twofold rotary translation (screw axis).[77] The unit cell thereby contains two asymmetric units related by this operation (Figure 1). The resulting monoclinic crystal's main feature are zigzag arrays of the hydrogen bonded OH-groups, with a O–O-distance of 2.8 Å and an OH···O angle of 168°. The aromatic rings are π-π-stacked with an inter-ring distance of 4.8 Å. The intramolecular geometry corresponds to a slightly positive puckering angle $\tau_1(C_9C_4C_3C_2)$ of 12°, that is, a pseudo equatorial conformation that is more planar than in the gas phase.[78–80] The crystallographic data are collected in Table S1.

The experimental IR absorption and VCD spectrum of (*S*)-(+)-1-indanol, measured in KBr, are shown as black curve in Figure 2. The VCD spectra of both enantiomers with the expected mirror image relation can be found in Figure S1; Figure 2 depicts the half difference between the two spectra. The IR absorption spectrum is dominated by three groups of intense bands that correspond to equally characteristic patterns in the VCD spectrum. The region above 1400 cm^{-1} stems from modes mainly described in terms of synchronous C_1H/OH bending and aromatic CC

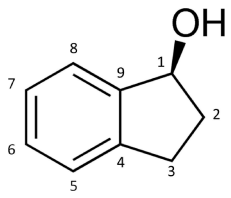

Scheme 1. (*S*)-(+)-1-Indanol with atom numbering.

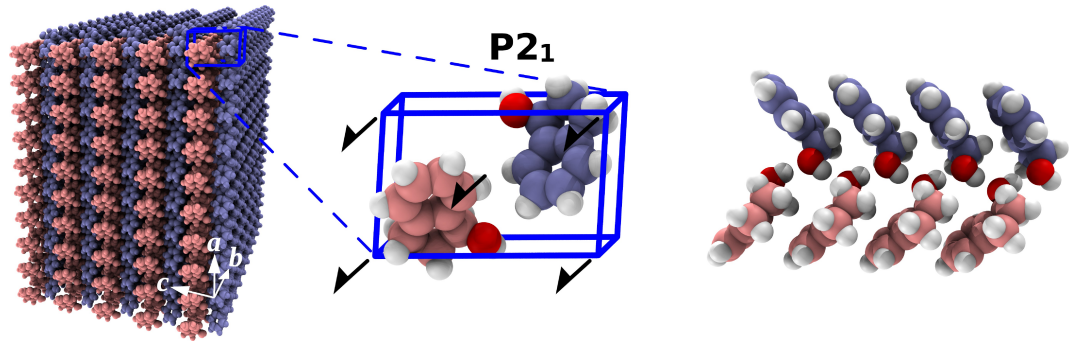

Figure 1. Crystal topology of (*S*)-(+)-1-indanol in Sohncke space group $P2_1$. The unit cell (middle) contains two molecules that transform into each other through a twofold screw axis. Molecules shown in the same colour are related through translation by the lattice vectors (left). The characteristic crystal feature is a zigzag array of hydrogen bonded OH-groups that can be taken as a reference for static calculations of a tetramer cluster (right, here shown as eight molecules).

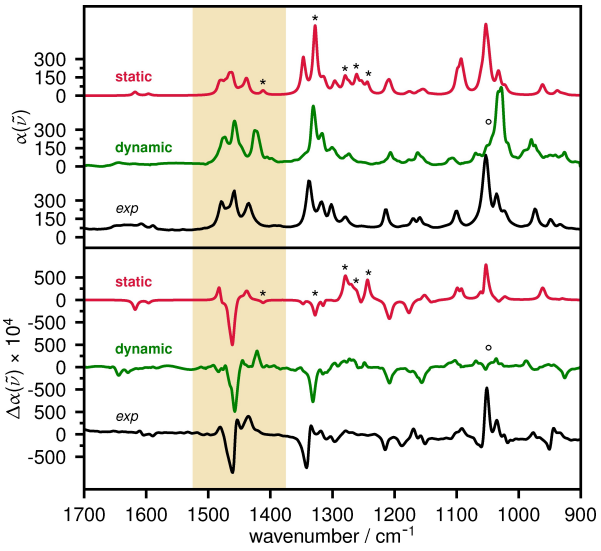

Figure 2. IR absorption (top) and VCD (bottom) spectra of (*S*)-(+)-1-indanol crystals: experimental data measured in KBr (black), AIMD-NVPT results of a fully periodic bulk crystal (green), and static Hessian-based calculations of a cluster model in gas phase (red). Asterisks mark peak artefacts that stem from boundary effects of the finite sample. Empty circles indicate the deficiency in the AIMD study in capturing the CO/CC stretch band correctly. See Figure 3 for a detailed analysis of the region marked in yellow.

stretching motions. The region 1200–1400 cm^{-1} involves mixed CH and CH_2 bending motions and that below 1200 cm^{-1} is dominated by the intense CC and CO stretch bands around 1050 cm^{-1}. The IR absorption in the solid state does not resemble the one in a non-polar solvent (CCl_4), but it is somewhat close to that measured in DMSO.[81] Consequently, the similarity of non-covalent interactions found in the solid and for a strongly polar solvent is sufficient to obtain comparable IR spectra, even though in solution crystal symmetry is absent. Most interestingly, this does not apply to the VCD spectrum, which is very different in the solid state from those in solution. In other words, mere inspection of the available experimental data points to the important role of crystal symmetry for the generation of VCD.

Recalling Rosenfeld's equation, VCD can be expressed as proportional to the product $\otimes$ (see the Supporting Information for the used notation) of the current and magnetic (transition) dipole moment, j and m:

written here in velocity form using the time-derivative of the electric dipole moment, μ, with $\mathrm{j} = \underline{\mu} = \frac{\partial}{\partial t}\mu$.[11,82] If we define the total dipole moments of the system in terms of a sum over individual molecular dipoles $\mathrm{j} = \sum_k \mathrm{j}_k$ and $\mathrm{m} = \sum_k \mathrm{m}_k$, we are able to distinguish local from non-local VCD:

$$\mathrm{j} \otimes \mathrm{m} = \underbrace{\sum_k \mathrm{j}_k \otimes \mathrm{m}_k}_{\text{local}} + \underbrace{\sum_k \sum_{l \neq k} \mathrm{j}_k \otimes \mathrm{m}_l}_{\text{non-local}} . \qquad (2)$$

The here presented calculations of solid-state VCD follow our recent work and rest on a fully periodic bulk crystal (2×2×1) and AIMD-NVPT calculations at DFT level (B3LYP-D3 and BLYP).[42,83–85] We compare the results with an often used, less computationally demanding cluster study via extraction of a characteristic crystal feature (cf., Figure 1, right) followed by static Hessian-based MFPT calculations (B3LYP-D3BJ/6-311++G(d,p)) (see the Supporting Information for computational details).[50,86] It is important to note that neglecting the crystal's periodicity in the static calculations does not only exclude all supramolecular interactions with crystal regions that are not contained in the cluster, but that it also alters the vibrational space due to the changed environment. Especially an incomplete hydrogen bond network entails unsaturated non-covalent interactions at the outer parts of the cluster (dangling bonds). Consequently, spectral artefacts can arise from both, the missing non-local interactions as well as the finite boundaries themselves.

The AIMD-NVPT calculations of IR absorption and VCD spectra are shown as green curves in Figure 2. Overall, the IR spectrum is in excellent agreement with the experiment, except for the CO/CC stretching band at 1050 cm^{-1} in

the experiment, which is misplaced by the calculations (see Table S2 for a detailed peak assignment). We observed a similar issue for this band in crystals of cyclohexanediol,[42] which probably arises from a deficiency of the functional in the AIMD. Expectedly, the good IR prediction materialises in VCD, (Figure 2 bottom, green curve), where the overall agreement with experiment is very good and the assignment of absolute configuration and crystal structure confirmation can be carried out unambiguously based on the calculations. The important deficiency in describing the CO/CC stretching band, however, continues in the VCD spectrum with the omission of the large positive peak found in experiment. Minor deficiencies appear just below 1200 and at 1300 cm^{-1}. Very noteworthy, in turn, is the good reproduction of the peak shoulder at 1425 cm^{-1}. The analysis of the subcrystalline space (cf., Figure S5) within the AIMD prediction reveals very important non-local contributions with peak intensities depending on coupled modes of more than one molecule in the crystal as will be discussed below. It furthermore suggests that already a tetramer cluster in the spirit of Figure 1 (right) reproduces large parts of the experimental IR absorption and VCD spectrum.

We therefore selected the tetramer cluster structure for the static Hessian-based reference calculations. The results are shown as red curves in Figure 2. The IR absorption is in satisfactory agreement with the experiment and can well reproduce the CO/CC stretch band around 1050 cm^{-1}. Only the region between 1240 and 1350 cm^{-1} is at odds with the experiment, in terms of intensities, and with additional peaks just below 1300 cm^{-1}. These are typical examples of artefacts that result from neglecting periodic boundary conditions in the computation of normal modes and linear response, leading to frequency shifts and peak splitting. The effect is strongest for modes that include dangling bonds at the boundaries, which is why especially the OH/CH bend region coupled with intense CH_2 wagging and twisting is affected the most, while it is negligible in other spectral regions. The static calculations for VCD predictions (Figure 2 bottom, red curve) justify using the tetramer model for this system as it is in overall good agreement with the experiment. The artefacts' marked presence, however, may obstruct the determination of crystal packing effects or polymorphism that relies on peak details beyond overall agreement. Generally, in regions of poor prediction of IR absorption, like in the region of artefacts (1240–1350 cm^{-1}), the prediction of VCD is unreliable, too. But an unambiguous assignment of the absolute configuration is possible and non-locality due to crystal packing is captured to some extent. Interestingly, the CO/CC stretch region, which is very well reproduced here, mainly consists of local VCD since it appears already in the monomer model (cf., Figure S5), and therefore does not stem from crystal packing. Care must be taken when non-local effects shall be studied by simply changing the cluster size, because for each subcluster fragment (monomer, dimer, etc.) a new Hessian has to be calculated. This renders frequencies and intensities size-dependent and subject to finite boundary effects, and predictions of non-locality eventually unreliable.

We have shown that the generation of non-local VCD patterns from delocalised modes can be much more subtle than in IR absorption.[41,42] This is due to the way these patterns emerge: The rotational strength, which defines VCD, is determined by the relative orientation of electric and magnetic (transition) dipole moments. However, the magnetic dipole moment is a pseudovector which depends on a reference origin, that is, the point in space where it is evaluated:

$$\mathrm{m}^{\mathcal{O}'} = \mathrm{m}^{\mathcal{O}} + \frac{1}{2c}(\mathcal{O} - \mathcal{O}') \times \mathrm{j}, \tag{3}$$

where $\mathcal{O}$ and $\mathcal{O}'$ correspond to different origins. If the non-local coupling of molecular electric and magnetic polarisation is to be considered, different regions of the system will be combined, and since a pseudovector is involved, the relative positions of the molecules involved will be relevant. This peculiar property of the rotational strength gives rise to direct coupling (DC) and gauge transport (GT) as two genuine terms of non-local VCD, with the origin-dependent part of the magnetic dipole moment being encoded in the GT term only (see the Supporting Information for a detailed derivation).[41,42,87,88]

Both terms, DC and GT, can be illustrated as in Scheme 2, which shows a system of two units (i.e., molecules). According to Equation (2), the overall polarisation of the system due to vibrational excitation can be described as electric and magnetic transition dipole moments localised in each molecule. When the vibrational transition is delocalised, the molecules oscillate collectively; moreover, a strong oscillation of one molecule can induce changes in the polarisation of a neighbouring molecule if they are strongly connected by non-covalent interactions, especially hydrogen bonds. In both cases, vibrational polarisation of one molecule alone does not sufficiently describe the observed spectra (local scope). The cross coupling between molecules can then be easily obtained by the combination of dipole moments of different units. For the direct coupling (DC) term, only the "intrinsic" moments of each unit are taken, that is, current (electric) dipole moments together with magnetic dipole moments that emerge in the local scope of each molecule. For the gauge transport (GT) term, the current (electric) dipole moment is combined with the magnetic dipole moment induced by the current of the other molecule at a chosen origin. Consequently, there is no GT term for IR absorption, because only current (electric) dipole moments, thus no pseudovectors, are combined here. DC and GT terms have been discussed in the past, especially by Nicu an co-workers[88] as well as Abbate[87] and co-workers. Traditionally, non-local VCD has been viewed through pure electric dipole-electric dipole contributions and the coupled oscillator (CO) model,[89] which is equivalent to the GT term described here. But already for signature systems like carbonyl oscillators, contributions from the ″intrinsic″ magnetic dipole moment, hence the DC term, turned out to be important.[87] Within the generalized CO (GCO) model, this term has been referred to as "correction term".[88,90]

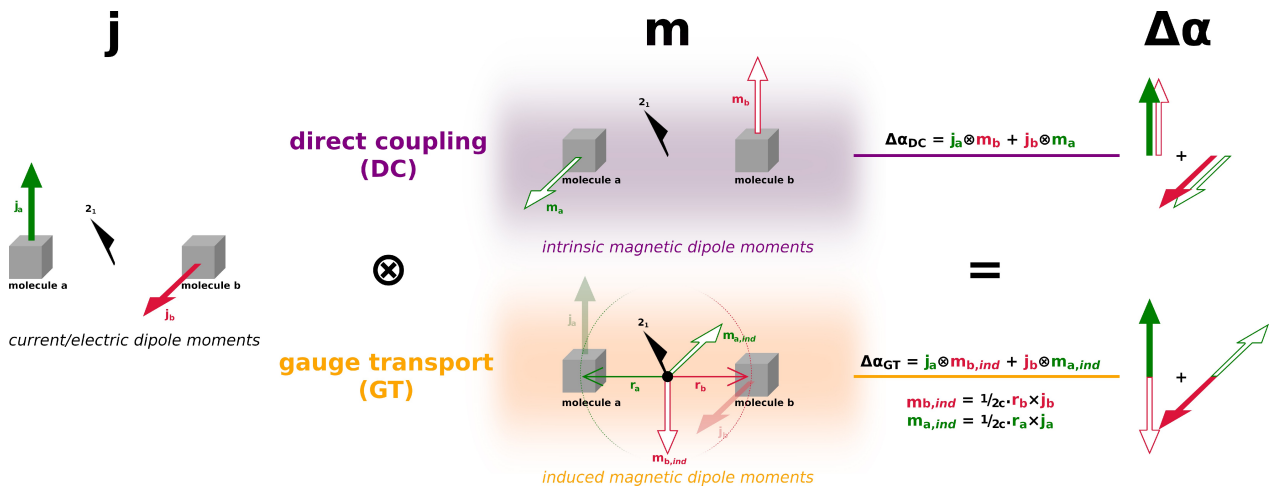

Scheme 2. Sketch illustrating the non-local terms of VCD: Local units (e.g., molecules) are shown as grey cubes and the twofold screw axis as a half-arrow (the displacement not shown for clarity). Vibrational excitation of the molecules results in electric (here in velocity form: current) and magnetic transition dipole moments, j and m, pointing in directions dictated by the orientation of the molecules. The rotational strength defining VCD is determined by the relative orientation of these moments. Current dipole moments are shown as full arrows, magnetic dipole moments as empty arrows. Upper panel: Direct coupling involving only the "intrinsic" dipole moments of the units, resulting in positive VCD for the shown example. Lower panel: Gauge transport describing the origin dependence of the magnetic dipole moment (chosen origin shown as a black dot), resulting in negative VCD for the shown example. Ultimately, the VCD spectrum does not depend on the choice of origin.[42] It is important to note that in the example shown, both terms give rise to new VCD peaks, which are absent in the local domain where only moments of the same unit are combined.

Although modern calculations often do not distinguish sharply between non-local DC and GT terms and local contributions to VCD, this becomes very important for the modelling of solid-state VCD.[42] First, because non-local terms adhere to the symmetry of the space group; their resolution thus provides deeper understanding of how crystal packing or specific solid-forms determine the spectrum. Second, because within periodic boundaries, the GT term requires special attention for the correct consideration of periodic images of units or molecules.[42]

It is worthwhile to take a closer look at how the $P2_1$ space group, however simple it appears, determines non-local VCD and imposes specific combination rules on the dipole moments. GT terms can only emerge from symmetry operations that include rotations, but not from simple translation, hence their range lies within the scope of one unit cell operation (here: 5 Å). The most peculiar effect of the single screw axis, however, is that it introduces an directionality into the DC terms: It supports the non-local combination of only sub-components of the dipole moments, that is, either parallel or orthogonal orientation with respect to the axis of rotation, but not both at the same time. With this selective quenching and enhancement of polarisation, DC terms can give rise to non-local peaks that are absent locally—and become as equally important as GT terms. The Supporting Information contains a comprehensive treatment of VCD terms under $P2_1$ crystal symmetry, wherefrom the directionality in the DC and GT terms can be deduced and the conditions for non-vanishing VCD be defined. Interestingly, these conditions are fulfilled only for certain bands in (*S*)-(+)-1-indanol, which directly connects crystal symmetry with the VCD spectrum.

Figure 3 (top) depicts the possible construction steps in order to form a $P2_1$ bulk crystal. Going from the level of individual molecules (units) that correspond to local IR and VCD signatures, two layered lattices can be defined through simple translation in two dimensions (shown in rose and blue, respectively). These layers transform with the 2_1 symmetry operation and eventually construct the complete crystal. The local and non-local IR and VCD spectra related to these construction steps are shown in Figure 3 (bottom) with special focus on the 1350–1550 cm^{-1} region. The results support the symmetry argument that GT terms can only arise for rotational symmetry operations and with this role it mediates between adjacent layers, yielding new non-local peaks. DC terms, in turn, appear for both operations, translation and screwing, whereas the former can only enhance (or decrease) what is present in the local scope. Again, it is the 2_1 operation that leads to novel peaks and underlines the complementary effect of the crystal structure on the VCD outcome. Interestingly, in the selected frequency range of Figure 3, DC and GT terms partially cancel leading to the peculiar peak shoulder between 1400 and 1450 cm^{-1} that is also found in the experiment, whereas there is hardly any change in the IR absorption spectrum. A depiction of the corresponding vibrational mode and bound polarisation can be found in Figure S7. This band is therefore a good example of the interplay of symmetry and polarisation leading to non-local VCD as explained in Scheme 2.

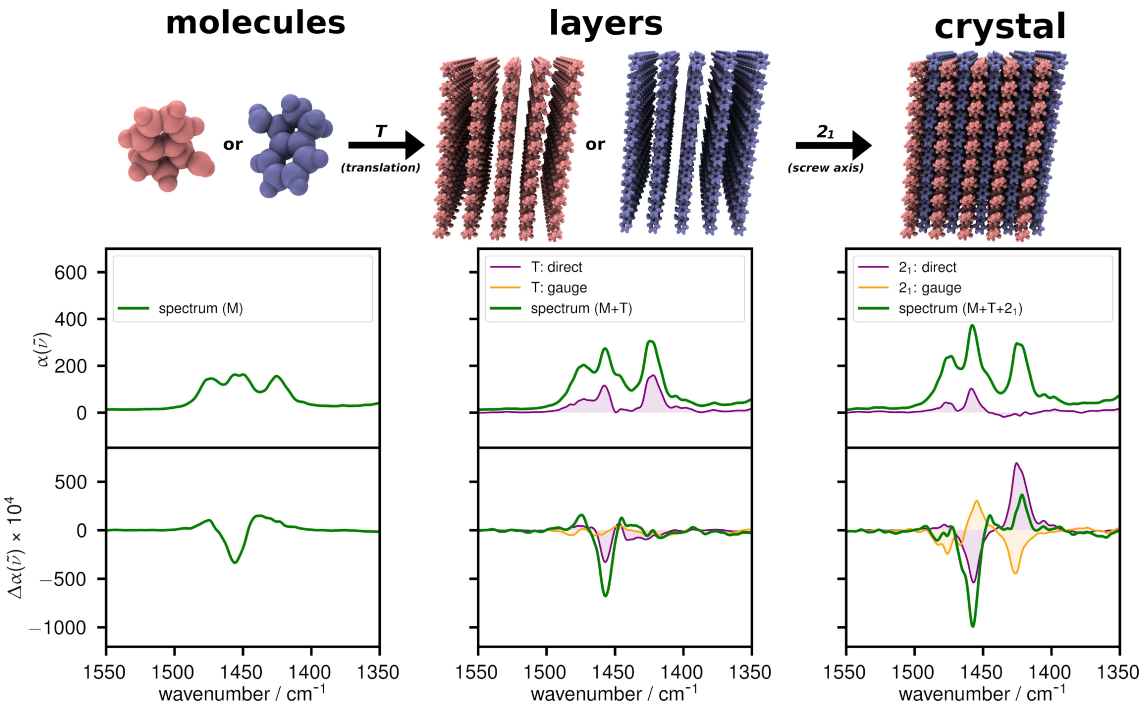

Figure 3. The emergence of non-local VCD in $P2_1$ crystals of (*S*)-(+)-1-indanol. The decomposition of the crystal following the point group's symmetry is shown together with the corresponding IR absorption and VCD (sub-)spectra from AIMD-NVPT calculations (frequency range according to marked region in Figure 2; for the full spectrum see Figure S6). Note that, while the analysis, being a post processing, is performed on individual molecules or layers, their dynamics and polarisation accounts for the presence of the entire crystal. Contributions stemming from direct coupling (DC) and gauge transport (GT) are shown in purple and yellow, respectively, while the full spectrum, which summarises all contributions from left to right is shown in green. Left: IR absorption and VCD from individual molecules correspond to the local scope; no non-local terms are defined. Centre: Layers, which are formed following the translation (T) symmetry of the space group, give rise to a non-vanishing DC term, while no GT term can be found (apart from noise). T-symmetry alone does not qualitatively change the IR or VCD spectrum found locally. Right: The 2D layers are connected through the twofold rotary-translation (2_1) operation of the space group. It is found that, by generating supramolecular chirality,[76] the 2_1 symmetry also leads to new non-local peaks due to symmetry-selective quenching or enhancement of polarisation. Note that there can no GT term be defined for IR absorption.

Conclusion

The presence of non-locality in solid-state VCD spectra is very common and by no means exceptional due to the intimate non-covalent connection of molecules in a crystal. Our results underline that also achiral space groups like $P2_1$ have the capacity to create important non-local VCD patterns. We illustrated by means of a combined experimental and theoretical study of (*S*)-(+)-1-indanol crystals how DC and GT terms equally contribute to VCD and that these terms figure integral parts of the solid-state spectrum. The chiral crystal's symmetry is directly conveyed to VCD through specific combination rules of (transition) dipole moments. GT terms are restricted to comparably short ranges in $P2_1$ groups (approx. 5 Å) since they do not result from translation, which is equivalent to two turns of the screw axis, impeding giant VCD enhancement. DC terms, in turn, reflect the directionality of the screw axis. We thus find that new VCD details emerge as soon as the chiral asymmetric unit is passed through the lattice, while the IR absorption spectrum does not change as much. These non-local VCD signals emerging from supramolecular chirality usually surpass the local signals, which makes VCD suitable for distinguishing polymorphic forms and other solid forms. With this, our work connects to preliminary investigations on structural chirality, but we find that the structural concepts of helicity do not simply translate into an equivalent concept of oscillator helicity since mode phase and relative orientation of polarisation vectors enter as additional factors.[36]

Our analysis is based on a fully periodic AIMD-NVPT study, but we compare the computational results to conventional static cluster calculations. Even though the cluster model lacks important peak details from the chiral crystal structure, it can reproduce the main VCD features and, in the case of (*S*)-(+)-1-indanol, even excels over AIMD in describing the CO stretching band. However, it misses important non-covalent interactions of the crystal leading to finite boundary effects that appear as significant peak artefacts in the spectrum. Hence, for comparably simple crystal symmetries, static cluster calculations can be used for the assignment of absolute configurations, but may come to their limits when the effect of the crystal packing or polymorphism shall be investigated. To these ends, the static approach has to be extended to fully periodic bulk crystal models, like it is used in the reference AIMD study. This would come with the advantage that one single point calculation sufficiently describes the conformational land-

scape due to the immobilisation of the molecules and that therefore a comparably high level of theory can be employed.

The thorough understanding of non-local VCD in solid state is still in an early stage, but it is going to enable the construction of crystal spectra from calculations of local units, which allows for a cost-effective analysis of large systems and supramolecular chirality.

Acknowledgements

This work was granted access to the HPC resources of IDRIS under the allocation 2021-100285 made by GENCI, as well as the Mésocentre computing center of Centrale Supélec and École Normale Supérieure Paris-Saclay supported by CNRS and Région Île-de-France. We thank Jérémy Lefèbvre for experimental help. This project has been funded by the French National Research Agency (ANR) (project: 18-CE29-0001-01), and by the Deutsche Forschungsgemeinschaft (DFG, German Research Foundation) (project: 451539523).

Conflict of Interest

There are no conflicts to declare.

Data Availability Statement

The data that support the findings of this study are openly available in Zenodo at https://doi.org/10.5281/zenodo.7228748, reference number 7228748.

Keywords: Ab Initio Molecular Dynamics · Chirality · Solid-State Spectroscopy · Vibrational Circular Dichroism

[1] W. H. Brooks, W. C. Guida, K. G. Daniel, *Curr. Top. Med. Chem.* **2011**, *11*, 760.
[2] M. Abram, M. Jakubiec, K. Kamiński, *ChemMedChem* **2019**, *14*, 1744.
[3] L.-F. Huang, W.-Q. T. Tong, *Adv. Drug Delivery Rev.* **2004**, *56*, 321.
[4] A. W. Newman, S. R. Byrn, *Drug Discovery Today* **2003**, *8*, 898.
[5] M. M. Quesada-Moreno, J. R. Aviles-Moreno, J. J. Lopez-Gonzalez, K. Jacob, L. Vendier, M. Etienne, I. Alkorta, J. Elguero, R. M. Claramunt, *Phys. Chem. Chem. Phys.* **2017**, *19*, 1632.
[6] *Comprehensive Chiroptical Spectroscopy* (Eds.: N. Berova, P. L. Polavarapu, K. Nakanishi, R. W. Woody), Wiley, Hoboken, **2012**.
[7] S. S. Wesolowski, D. E. Pivonka, *Bioorg. Med. Chem. Lett.* **2013**, *23*, 4019.
[8] M. Krupová, P. Leszczenko, E. Sierka, S. E. Hamplová, R. Pelc, V. Andrushchenko, *Chem. Eur. J.* **2022**, *28*, e202201922.
[9] L. A. Nafie, *Chirality* **2020**, *32*, 667.
[10] M. Krupová, J. Kessler, P. Bouř, *ChemPlusChem* **2020**, *85*, 561.
[11] L. A. Nafie, *Vibrational Optical Activity: Principles and Applications*, Wiley, Hoboken, **2011**.
[12] P. J. Stephens, F. J. Devlin, J.-J. Pan, *Chirality* **2008**, *20*, 643.
[13] X. Li, M. Porcino, C. Martineau-Corcos, T. Guo, T. Xiong, W. Zhu, G. Patriarche, C. Péchoux, B. Perronne, A. Hassan, R. Kümmerle, A. Michelet, A. Zehnacker-Rentien, J. Zhang, R. Gref, *Int. J. Pharm.* **2020**, *585*, 119442.
[14] C. Merten, *Eur. J. Org. Chem.* **2020**, 5892.
[15] P. L. Polavarapu, E. Santoro, *Nat. Prod. Rep.* **2020**, *37*, 1661.
[16] A. Bouchet, T. Brotin, D. Cavagnat, T. Buffeteau, *Chem. Eur. J.* **2010**, *16*, 4507.
[17] S. Ma, X. Cao, M. Mak, A. Sadik, C. Walkner, T. B. Freedman, I. K. Lednev, R. K. Dukor, L. A. Nafie, *J. Am. Chem. Soc.* **2007**, *129*, 12364.
[18] C. Gautier, T. Bürgi, *ChemPhysChem* **2009**, *10*, 483.
[19] J. Ouyang, A. Swartjes, M. Geerts, P. J. Gilissen, D. Wang, P. C. P. Teeuwen, P. Tinnemans, N. Vanthuyne, S. Chentouf, F. P. J. T. Rutjes, J.-V. Naubron, J. Crassous, J. A. A. W. Elemans, R. J. M. Nolte, *Nat. Commun.* **2020**, *11*, 4776.
[20] H. Sato, A. Yamagishi, M. Shimizu, K. Watanabe, J. Koshoubu, J. Yoshida, I. Kawamura, *J. Phys. Chem. Lett.* **2021**, *12*, 7733.
[21] H. Sato, K. Tamura, K. Takimoto, A. Yamagishi, *Phys. Chem. Chem. Phys.* **2018**, *20*, 3141.
[22] T. A. Keiderling, *Chem. Rev.* **2020**, *120*, 3381.
[23] H. Sato, I. Kawamura, *Biochim. Biophys. Acta Proteins Proteomics* **2020**, *1868*, 140439.
[24] V. Declerck, A. Pérez-Mellor, R. Guillot, D. J. Aitken, M. Mons, A. Zehnacker, *Chirality* **2019**, *31*, 547.
[25] A. Pérez-Mellor, A. Zehnacker, *Chirality* **2017**, *29*, 89.
[26] P. Novotná, M. Urbanová, *Chirality* **2015**, *27*, 965.
[27] Y.-K. Chao, N. M. Praveena, K.-C. Yang, E. B. Gowd, R.-M. Ho, *Soft Matter* **2022**, *18*, 2722.
[28] M. A. J. Koenis, V. P. Nicu, L. Visscher, C. Kuehn, M. Bremer, M. Krier, H. Untenecker, U. Zhumaev, B. Küstner, W. J. Buma, *Phys. Chem. Chem. Phys.* **2021**, *23*, 10021.
[29] M. A. J. Koenis, A. Osypenko, G. Fuks, N. Giuseppone, V. P. Nicu, L. Visscher, W. J. Buma, *J. Am. Chem. Soc.* **2020**, *142*, 1020.
[30] H. Sato, *Phys. Chem. Chem. Phys.* **2020**, *22*, 7671.
[31] J. Dupont, R. Guillot, V. Lepère, A. Zehnacker, *J. Mol. Struct.* **2022**, *1262*, 133059.
[32] J. E. Rode, K. Lyczko, K. Kosińska, J. Matalińska, J. Dyniewicz, A. Misicka, J. C. Dobrowolski, P. F. Lipiński, *Spectrochim. Acta Part A* **2022**, *269*, 120761.
[33] A. Pérez-Mellor, K. L. Barbu-Debus, A. Zehnacker, *Chirality* **2020**, *32*, 693.
[34] M. M. Quesada-Moreno, A. J. Cruz-Cabeza, J. R. Avilés-Moreno, P. Cabildo, R. M. Claramunt, I. Alkorta, J. Elguero, F. J. Zúñiga, J. J. López-González, *J. Phys. Chem. A* **2017**, *121*, 5665.
[35] H. Sato, T. Yajima, A. Yamagishi, *Chirality* **2015**, *27*, 659.
[36] T. Sasaki, I. Hisaki, T. Miyano, N. Tohnai, K. Morimoto, H. Sato, S. Tsuzuki, M. Miyata, *Nat. Commun.* **2013**, *4*, 1787.
[37] T. Sasaki, M. Miyata, H. Sato, *Cryst. Growth Des.* **2018**, *18*, 4621.
[38] P. Rizzo, M. Beltrani, G. Guerra, *Chirality* **2010**, *22*, E67.
[39] J. Frelek, M. Górecki, A. Dziedzic, E. Jabłońska, B. Kamieński, R. K. Wojcieszczyk, R. Luboradzki, W. J. Szczepek, *J. Pharmacol. Sci.* **2015**, *104*, 1650.
[40] J. Frelek, M. Górecki, M. Łaszcz, A. Suszczyńska, E. Vass, W. J. Szczepek, *Chem. Commun.* **2012**, *48*, 5295.
[41] S. Jähnigen, A. Scherrer, R. Vuilleumier, D. Sebastiani, *Angew. Chem. Int. Ed.* **2018**, *57*, 13344; *Angew. Chem.* **2018**, *130*, 13528.
[42] S. Jähnigen, A. Zehnacker, R. Vuilleumier, *J. Phys. Chem. Lett.* **2021**, *12*, 7213.

[43] C. Merten, T. Kowalik, A. Hartwig, *Appl. Spectrosc.* **2008**, *62*, 901.
[44] T. Buffeteau, F. Lagugné-Labarthet, C. Sourisseau, *Appl. Spectrosc.* **2005**, *59*, 732.
[45] B. Z. Chowdhry, T. J. Dines, S. Jabeen, R. Withnall, *J. Phys. Chem. A* **2008**, *112*, 10333.
[46] H. Sato, I. Kawamura, A. Yamagishi, F. Sato, *Chem. Lett.* **2017**, *46*, 449.
[47] N. Jiang, R. X. Tan, J. Ma, *J. Phys. Chem. B* **2011**, *115*, 2801.
[48] K. Ishikawa, Y. Terasawa, M. Tanaka, T. Asahi, *J. Phys. Chem. Solids* **2017**, *104*, 257.
[49] P. J. Stephens, *J. Phys. Chem.* **1985**, *89*, 748.
[50] J. Cheeseman, M. Frisch, F. Devlin, P. Stephens, *Chem. Phys. Lett.* **1996**, *252*, 211.
[51] L. A. Nafie, T. B. Freedman, *J. Chem. Phys.* **1983**, *78*, 7108.
[52] A. Scherrer, F. Agostini, D. Sebastiani, E. K. U. Gross, R. Vuilleumier, *J. Chem. Phys.* **2015**, *143*, 074106.
[53] V. P. Nicu, J. Neugebauer, S. K. Wolff, E. J. Baerends, *Theor. Chem. Acc.* **2008**, *119*, 245.
[54] K. Reiter, M. Kühn, F. Weigend, *J. Chem. Phys.* **2017**, *146*, 054102.
[55] A. Scherrer, R. Vuilleumier, D. Sebastiani, *J. Chem. Theory Comput.* **2013**, *9*, 5305.
[56] A. Scherrer, R. Vuilleumier, D. Sebastiani, *J. Chem. Phys.* **2016**, *145*, 084101.
[57] E. Ditler, T. Zimmermann, C. Kumar, S. Luber, *J. Chem. Theory Comput.* **2022**, *18*, 2448.
[58] L. Paoloni, G. Mazzeo, G. Longhi, S. Abbate, M. Fusè, J. Bloino, V. Barone, *J. Phys. Chem. A* **2020**, *124*, 1011.
[59] J. Bloino, M. Biczysko, V. Barone, *J. Phys. Chem. A* **2015**, *119*, 11862.
[60] C. Cappelli, J. Bloino, F. Lipparini, V. Barone, *J. Phys. Chem. Lett.* **2012**, *3*, 1766.
[61] C. Merten, J. Bloino, V. Barone, Y. Xu, *J. Phys. Chem. Lett.* **2013**, *4*, 3424.
[62] M. Thomas, B. Kirchner, *J. Phys. Chem. Lett.* **2016**, *7*, 509.
[63] B. Kirchner, J. Blasius, L. Esser, W. Reckien, *Adv. Theory Simul.* **2021**, *4*, 2000223.
[64] S. Jähnigen, D. Sebastiani, R. Vuilleumier, *Phys. Chem. Chem. Phys.* **2021**, *23*, 17232.
[65] C. Qu, J. M. Bowman, *Phys. Chem. Chem. Phys.* **2019**, *21*, 3397.
[66] R. Ramírez, T. López-Ciudad, P. Kumar, D. Marx, *J. Chem. Phys.* **2004**, *121*, 3973.
[67] M. Basire, F. Mouhat, G. Fraux, A. Bordage, J.-L. Hazemann, M. Louvel, R. Spezia, S. Bonella, R. Vuilleumier, *J. Chem. Phys.* **2017**, *146*, 134102.
[68] M.-P. Gaigeot, M. Martinez, R. Vuilleumier, *Mol. Phys.* **2007**, *105*, 2857.
[69] M. Thomas, M. Brehm, R. Fligg, P. Vohringer, B. Kirchner, *Phys. Chem. Chem. Phys.* **2013**, *15*, 6608.
[70] E. Ditler, S. Luber, *WIREs Comput. Mol. Sci.* **2022**, *12*, e1605.
[71] S. Abbate, G. Longhi, K. Kwon, A. Moscowitz, *J. Chem. Phys.* **1998**, *108*, 50.
[72] R. Kubo, *J. Phys. Soc. Jpn.* **1957**, *12*, 570.
[73] S. Jähnigen, "ChirPy" A python package for chirality, dynamics, and molecular vibrations (version 0.23.2); https://github.com/sjaehnigen/chirpy, Zenodo **2022**, 4775330.
[74] T. Rekis, *Acta Crystallogr. Sect. B* **2020**, *76*, 307.
[75] C. Dryzun, D. Avnir, *Chem. Commun.* **2012**, *48*, 5874.
[76] M. Miyata, N. Tohnai, I. Hisaki, T. Sasaki, *Symmetry* **2015**, *7*, 1914.
[77] Deposition Number 2077885 contains the supplementary crystallographic data for this paper. These data are provided free of charge by the joint Cambridge Crystallographic Data Centre and Fachinformationszentrum Karlsruhe Access Structures service.
[78] J. Altnöder, A. Bouchet, J. J. Lee, K. E. Otto, M. A. Suhm, A. Zehnacker-Rentien, *Phys. Chem. Chem. Phys.* **2013**, *15*, 10167.
[79] A. Bouchet, J. Altnöder, M. Broquier, A. Zehnacker, *J. Mol. Struct.* **2014**, *1076*, 344.
[80] K. Le Barbu-Debus, F. Lahmani, A. Zehnacker-Rentien, N. Guchhait, S. S. Panja, T. Chakraborty, *J. Chem. Phys.* **2006**, *125*, 174305.
[81] K. Le Barbu-Debus, A. Scherrer, A. Bouchet, D. Sebastiani, R. Vuilleumier, A. Zehnacker, *Phys. Chem. Chem. Phys.* **2018**, *20*, 14635.
[82] S. Heislbetz, G. Rauhut, *J. Chem. Phys.* **2010**, *132*, 124102.
[83] T. D. Kühne, M. Iannuzzi, M. Del Ben, V. V. Rybkin, P. Seewald, F. Stein, T. Laino, R. Z. Khaliullin, O. Schütt, F. Schiffmann, D. Golze, J. Wilhelm, S. Chulkov, M. H. Bani-Hashemian, V. Weber, U. Borstnik, M. Taillefumier, A. S. Jakobovits, A. Lazzaro, H. Pabst, T. Müller, R. Schade, M. Guidon, S. Andermatt, N. Holmberg, G. K. Schenter, A. Hehn, A. Bussy, F. Belleflamme, G. Tabacchi, A. Glöß, M. Lass, I. Bethune, C. J. Mundy, C. Plessl, M. Watkins, J. VandeVondele, M. Krack, J. Hutter, *J. Chem. Phys.* **2020**, *152*, 194103.
[84] A. D. Becke, *J. Chem. Phys.* **1993**, *98*, 5648.
[85] S. Grimme, J. Antony, S. Ehrlich, H. Krieg, *J. Chem. Phys.* **2010**, *132*, 154104.
[86] S. Grimme, S. Ehrlich, L. Goerigk, *J. Comput. Chem.* **2011**, *32*, 1456.
[87] S. Abbate, T. Bruhn, G. Pescitelli, G. Longhi, *J. Phys. Chem. A* **2017**, *121*, 394.
[88] V. P. Nicu, *Phys. Chem. Chem. Phys.* **2016**, *18*, 21202.
[89] G. Holzwarth, I. Chabay, *J. Chem. Phys.* **1972**, *57*, 1632.
[90] M. A. J. Koenis, O. Visser, L. Visscher, W. J. Buma, V. P. Nicu, *J. Chem. Inf. Model.* **2020**, *60*, 259.

Manuscript received: October 23, 2022
Accepted manuscript online: November 28, 2022
Version of record online: ■■, ■■

Research Articles

Chirality

S. Jähnigen,* K. Le Barbu-Debus, R. Guillot, R. Vuilleumier, A. Zehnacker* **e202215599**

How Crystal Symmetry Dictates Non-Local Vibrational Circular Dichroism in the Solid State

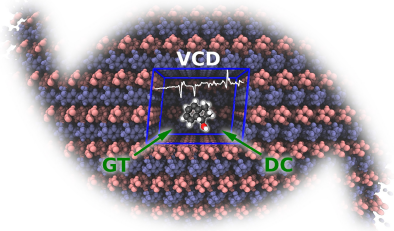

Solid-State Vibrational Circular Dichroism (VCD) is intimately linked to crystal symmetry and therefore has the capability to distinguish between polymorphic forms. In this article, we classify the non-local terms due to crystal chirality versus the local terms due to molecular chirality. We find that already an achiral screw axis leads to significant changes in the VCD spectrum that are intrinsic to the crystal structure.